Hydrogen Produced from Hydrohalic Acid Solutions by a Two-Electron Mixed-Valence Photocatalyst

Alan F. Heyduk and Daniel G. Nocera*

Energy conversion cycles are aimed at driving unfavorable, small-molecule activation reactions with a photon harnessed by a transition metal complex. A challenge that has occupied researchers for several decades is to create molecular photocatalysts to promote the production of hydrogen from homogeneous solution. We now report the use of a two-electron mixed-valence dirhodium compound to photocatalyze the reduction of hydrohalic acid to hydrogen. In this cycle, photons break two Rh^{II}–X bonds of a LRh^0–$Rh^{II}X_2$ core in the presence of a halogen trap to regenerate the active LRh^0–Rh^0 catalyst, which reacts with hydrohalic acid to produce hydrogen.

Light-driven energy conversion schemes were suggested as an alternative energy source to expendable fossil fuel reserves nearly a century ago (*1*). The target fuel of schemes developed since this proposal has been H_2, generated from protic solutions. The most successful approaches to date have used a heterogeneous catalyst to couple the $1e^-$ equivalency provided by a photoexcited transition metal sensitizer [e.g., Ru(II) polypyridine complexes] to the $2e^-$ equivalency required for H_2 production (*2*–*5*). Photoexcited electrons in the conduction bands of semiconducting electrodes and nanoparticles are especially effective in promoting the reduction of H^+ to H_2 (*6*, *7*). Utilization of the attendant hole in the valence band to generate a complementary oxidation product completes the photocatalytic cycle. Sutin and co-workers (*8*) showed that photocatalytic H_2 production in homogeneous solution could also be achieved when the heterogeneous mediator is replaced by a molecule capable of mediating the $2e^-$ reduction of 2 H^+ to H_2.

Hydrogen production in the absence of mediators has also been realized, but only under stoichiometric conditions. The irradiation of acidic solutions containing reduced metal ions such as Ce^{3+} (*9*), Cr^{2+} (*10*), and Fe^{2+} (*11*) produces H_2 and the $1e^-$ oxidized metal cation. In these schemes, excitation of a charge-transfer–to–solvent (CTTS) absorption band effectively produces solvated electrons that are trapped by protons to produce H radicals, which combine to produce H_2. The seminal work of Gray and co-workers on the photochemistry of dirhodium(I) isocyanides in hydrohalic acid (HX) solutions (*12*, *13*) established the viability of using a molecular excited state to promote H_2 production in homogeneous solution. Irradiation of the binuclear Rh^I complex, $[Rh_2(bridge)_4]^{2+}$ (bridge = 1,3-diisocyanopropane), in aqueous HX solutions resulted in the stoichiometric production of 1 equivalent (equiv) of H_2 and 1 equiv of $[Rh_2(bridge)_4Cl_2]^{2+}$. The difficulty associated with the subsequent activation of the Rh^{II}–X bonds of the $[Rh_2(bridge)_4Cl_2]^{2+}$ photoproduct prevented the regeneration of the initial photoreagent, precluding catalytic turnover.

In view of the challenges posed by M–X bond formation to designing HX-splitting cycles, we sought to develop excited states that can promote M–X photoactivation to regenerate active hydrogen-producing species. By introducing the same $d\sigma^*$ excited state within the electronic structure of LRh^0–Rh^0L, LRh^0–$Rh^{II}X_2$, and X_2Rh^{II}–$Rh^{II}X_2$ cores (X = Cl, Br; L = CO, PR_3, CNR) spanned by three bis(difluorophosphino) methylamine [dfpma = $MeN(PF_2)_2$] ligands (*14*, *15*), we could interconvert among the series members by photoeliminating halogen in $2e^-$ steps. We obtained the mixed-valence LRh^0–$Rh^{II}X_2$ species, $Rh_2(dfpma)_3X_2(L)$, quantitatively when solutions of $Rh_2(dfpma)_3X_4$ containing excess L were photolyzed (300 nm $\leq \lambda_{exc} \leq$ 480 nm) in the presence of a halogen-atom trap such as tetrahydrofuran (THF), dihydroanthracene, or 2,3-dimethylbutadiene. Irradiation with excitation wavelengths (300 nm $\leq \lambda_{exc} \leq$ 400 nm) coincident with the absorption manifold of the LRh^0–$Rh^{II}X_2$ photoproduct resulted in a second $2e^-$ elimination reaction to give the LRh^0–Rh^0L dimer, $Rh_2(dfpma)_3L_2$, again in quantitative yield. In the overall transformation, the two-electron mixed-valence LRh^0–$Rh^{II}X_2$ compound sustains the multielectron photoreactivity of the system by coupling the $2e^-$ M–X chemistry of the individual Rh centers. We now show that M–X photoactivation from this two-electron mixed-valence platform enables the photocatalytic production of H_2 from homogeneous solutions of HX.

Hydrohalic acid reacted at the $Rh_2^{0,0}(dfpma)_3(L)$ core to produce the two-electron mixed-valence species $Rh_2^{0,II}(dfpma)_3X_2(L)$ (**1**) and H_2 upon removal of a single axial ligand from the coordinatively saturated $Rh_2^{0,0}(dfpma)_3LL'$ (**2**) complex (Scheme 1). The vacant coordination site can be generated photochemically when one axial ligand is CO. We prepared the asymmetric complex, $Rh_2^{0,0}(dfpma)_3(PPh_3)(CO)$ (*16*), which has one photoinert axial ligand, PPh_3, and one photolabile axial ligand, CO. Whereas CH_2Cl_2 solutions of $Rh_2^{0,0}(dfpma)_3(PPh_3)(CO)$ did not react with HX (X = Cl or Br), a rapid reaction was observed when the CO was removed by ultraviolet-visible (UV-Vis) irradiation (excitation wavelength $\lambda_{exc} \geq$ 338 nm) (*17*). The spectral changes for the HCl reaction are displayed in Fig. 1. The final absorption profile is identical to that of $Rh_2^{0,II}(dfpma)_3Cl_2(PPh_3)$, which was obtained in quantitative yield. Ex-

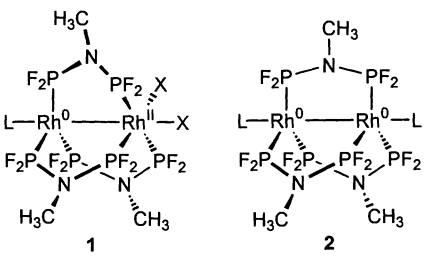

Scheme 1.

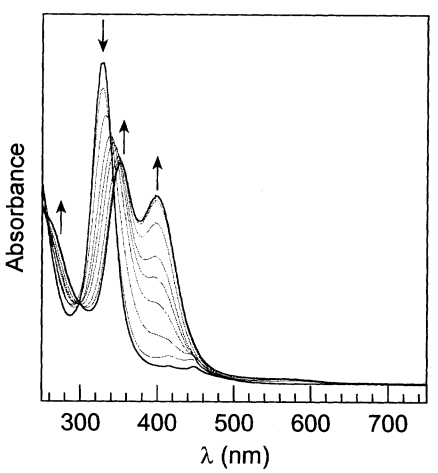

Fig. 1. Changes in the electronic absorption spectrum during photolysis. UV-Vis photolysis ($\lambda_{exc} \geq$ 338 nm) of $Rh_2(dfpma)_3(CO)(PPh_3)$ in 0.1 M HCl/CH_2Cl_2 solution at 20°C. The sample was irradiated for a total of 25 min. Arrows denote the evolution of the absorption spectrum with time.

Department of Chemistry, 6-335, Massachusetts Institute of Technology, Cambridge, MA 02139–4307, USA.

*To whom correspondence should be addressed. E-mail: nocera@mit.edu

periments in which a Toepler pump was used to collect H_2 show the formation of 0.87 ± 0.14 equiv of H_2 gas per 1.0 equiv of metal complex (*18*, *19*), establishing the overall stoichiometry of the reaction to be

$$Rh_2^{0,0}(dfpma)_3(CO)(PPh_3) + 2HX \xrightarrow[-CO]{h\nu\ (\lambda \geq 338\ nm)} Rh_2^{0,II}(dfpma)_3X_2(PPh_3) + H_2 \quad (1)$$

Wavelength selection of the excitation light reveals that H_2 is produced in a stepwise reaction sequence. Irradiation of $Rh_2^{0,0}$-$(dfpma)_3(CO)(PPh_3)$ in a 0.1 M HCl/THF solution with λ_{exc} = 335 nm led to changes in the UV-Vis absorption spectrum (Fig. 2A). Disappearance of the $Rh_2^{0,0}(dfpma)_3(PPh_3)$-(CO) absorption features was accompanied by the growth of an absorption band centered at 580 nm. The reaction proceeds smoothly with isosbestic points maintained at 296 and 338 nm. After 90 min of irradiation, no further changes were observed in the 580-nm absorption band; 0.35 ± 0.07 equiv of H_2 was produced during this photoconversion. The 580-nm absorption profile did not change with continued irradiation, nor did its intensity change for solutions stored in the dark. Although the 580-nm intermediate has not been isolated and characterized, its spectral profile is a signature of a tetranuclear Rh cluster with mixed-valence character (*20*–*23*). As observed by Gray and co-workers in their studies of $[Rh_2\ bridge)_4]^{2+}$ (*20*), a tetranuclear Rh species can result from the bimolecular reaction of two hydrido-halo dirhodium cores to produce 1 equiv of H_2 and a tetranuclear species (0.5 equiv of H_2 per equiv of Rh_2 complex). When the excitation wavelength is changed to frequencies within the spectral envelope of the 580-nm band, the absorbance decreases with the concomitant appearance of the two-electron mixed-valence dihalide, $Rh_2^{0,II}(dfpma)_3Cl_2(PPh_3)$ (Fig. 2B). Consistent with the overall stoichiometry of Eq. 1, Toepler pumping revealed that the remaining 0.38 ± 0.07 equiv of H_2 was produced upon conversion to the final LRh^0–$Rh^{II}X_2$ photoproduct.

Because the LRh^0–Rh^0 species can be regenerated by photolysis of $Rh_2^{0,II}$-$(dfpma)_3X_2(PPh_3)$ in the presence of halogen-atom traps (*14*, *15*), the reaction of Eq. 1 can be turned over and H_2 can be photocatalytically generated. A 50-ml THF solution containing $Rh_2^{0,II}(dfpma)_3Cl_2(PPh_3)$ (0.95 μmol) and 0.1 M HCl was irradiated with $\lambda_{exc} \geq 338$ nm, after which the photolysis was halted and H_2 was collected by Toepler pumping (*24*). Figure 3 displays the plot of total H_2 production versus time; an initial rate of 27 turnovers per hour was observed during the initial 3 hours of irradiation. The decrease in rate of H_2 production with continued photolysis was accompanied by a steady decrease in the $Rh_2^{0,II}(dfpma)_3Cl_2(PPh_3)$ absorbance, indicating the decomposition of the two-electron mixed-valence dimer. Preliminary investigations indicate that this decomposition product is a Rh monomer. When the photoreaction was performed with monochromatic excitation at 335 nm, the foregoing 580-nm intermediate was observed. Under these conditions, subsequent irradiation into the 580-nm absorption band was needed to turn the reaction over.

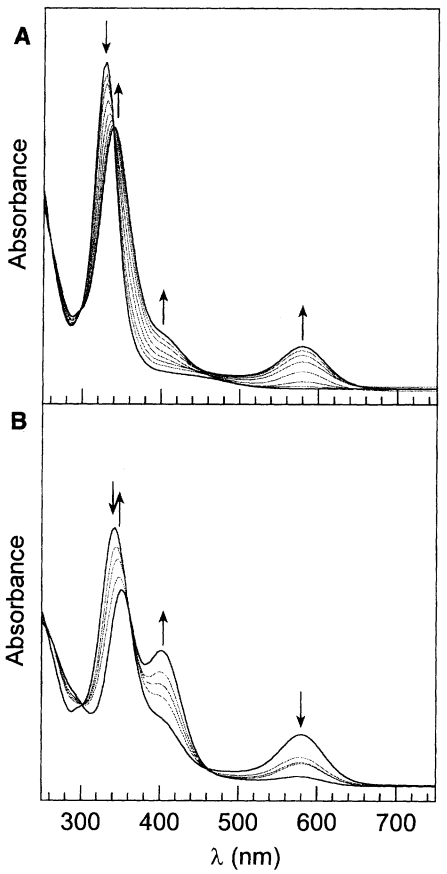

Fig. 2. Changes in the electronic absorption spectrum during photolysis. **(A)** Monochromatic UV photolysis (λ_{exc} = 335 nm) of $Rh_2(dfpma)_3(CO)(PPh_3)$ in 0.1 M HCl/THF solution at 20°C. The sample was irradiated for a total of 90 min. **(B)** Continued visible photolysis of the solution of (A) with long-pass filtered excitation light ($\lambda_{exc} \geq 338$ nm). Arrows denote the evolution of the absorption spectrum with time.

The above results are consistent with the catalytic cycle shown in Scheme 2. Per Toepler pump experiments, HX reacts with a coordinatively unsaturated LRh^0–Rh^0 core to produce H_2 (0.5 equiv per Rh_2 complex) and the blue intermediate, which we tentatively ascribe to a tetranuclear Rh species. This intermediate species is photochemically stable in the absence of visible-light irradiation, but a 580-nm photon prompts reaction to give 2 equiv of the LRh^0–$Rh^{II}X_2$ mixed-valence complex with the generation of an additional equivalent of H_2. The near-UV irradiation of the two-electron mixed-valence photoproduct in the presence of a halogen-atom trap regenerates LRh^0–Rh^0, which is available to react with HX to turn the cycle over.

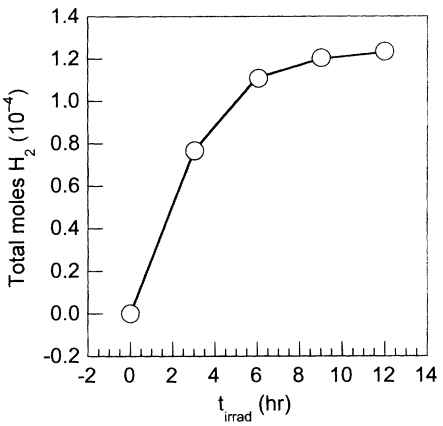

Fig. 3. The plot of total H_2 collected as a function of time for the UV-Vis white-light irradiation ($\lambda_{exc} \geq 338$ nm) of $Rh_2(dfpma)_3Cl_2(PPh_3)$ in 0.1 M HCl/THF solution at 20°C.

We believe that the two-electron mixed-valence character of the dihalide species is crucial to the overall reactivity. Reductive elimination from Rh_2 cores is facile when a Rh–Rh bond is preserved (*25*, *26*). In Scheme 2, the LRh^0–Rh^0L species contains a metal-metal bond that is characteristic of the pairing of electrons within the $d_{z^2}\sigma$ orbital of a d^9–d^9 core (*27*). As we have established computationally and spectroscopically (*14*), the same Rh–Rh bond interaction arises from the pairing of electrons in the d_{z^2} orbitals of a d^7–d^9 core of a LRh^0–$Rh^{II}X_2$ complex. Consequently, a Rh–Rh bond is maintained upon X elimination, a situation that does not arise for valence-symmetric binuclear Rh cores, including that of $[Rh_2(bridge)_4Cl_2]^{2+}$. This distinguishing trait of the two-electron mixed-valence core may be crucial to the smooth conversion of $Rh_2^{0,II}(dfpma)_3X_2(L)$ to $Rh_2^{0,0}(dfpma)_3L$, thus enabling turnover to be achieved.

Scheme 2 constitutes a photocatalytic HX-splitting cycle that is driven by halogen-atom trapping. An authentic energy-storing cycle demands the isolation of X_2 in the absence of a halogen-trapping reagent. The key to achieving this objective is intimately tied to the M–X photoelimination step. That the activation of the Rh–X bond is determinant to overall photocatalytic activity of Scheme 2 is established by the rate of H_2 production, which is commensurate with the quantum efficiency for the stoichiometric conversion of $Rh_2^{0,II}(dfpma)_3Cl_2(L)$ to $Rh_2^{0,0}(dfpma)_3L_2$ [$\phi_p = 6 \times 10^{-3}$ (*15*)]. This result highlights that an increased understanding of M–X photoactivation processes is imperative to the development of an energy conversion photocatalyst at the molecular level.

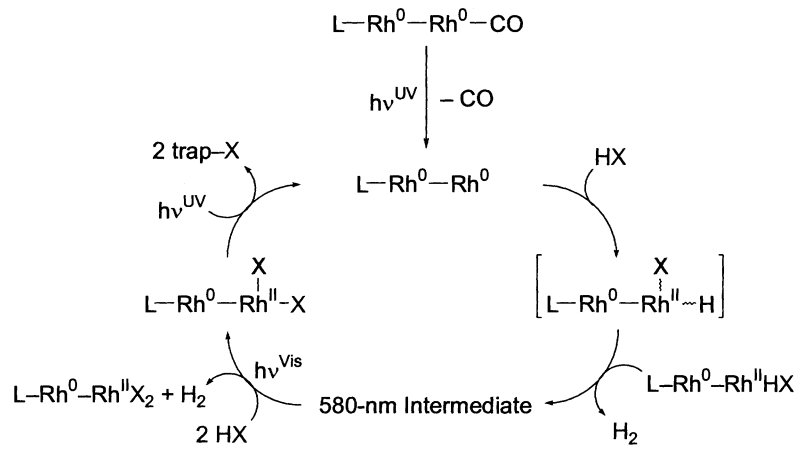

Scheme 2.

References and Notes

1. G. Ciamician, *Science* **36**, 385 (1912).
2. M. Grätzel, Ed., *Energy Resources Through Photochemistry and Catalysis* (Academic Press, New York, 1983).
3. M. A. Fox, M. Chanon, Eds., *Photoinduced Electron Transfer* (Elsevier, Amsterdam, 1988), parts A to D.
4. J. R. Norris Jr., D. Meisel, Eds., *Photochemical Energy Conversion* (Elsevier, New York, 1989).
5. N. Sutin, C. Creutz, E. Fujita, *Comm. Inorg. Chem.* **19**, 67 (1997).
6. A. Hagfeldt, M. Grätzel, *Acc. Chem. Res.* **33**, 269 (2000).
7. M. Grätzel, J.-E. Moser, in *Electron Transfer in Chemistry*, V. Balzani, Ed. (Wiley-VCH, Weinheim, Germany, 2001), vol. 5, part 3, chap. 1, pp. 589–644.
8. G. M. Brown, B. S. Brunschwig, C. Creutz, J. F. Endicott, N. Sutin, *J. Am. Chem. Soc.* **101**, 1298 (1979).
9. L. J. Heidt, A. F. McMillan, *J. Am. Chem. Soc.* **76**, 2135 (1954).
10. E. Collinson, F. S. Dainton, M. A. Malati, *Trans. Faraday Soc.* **55**, 2096 (1959).
11. L. J. Heidt, M. G. Mullin, W. B. Martin, A. J. M. Beatty, *J. Phys. Chem.* **66**, 336 (1962).
12. K. R. Mann *et al.*, *J. Am. Chem. Soc.* **99**, 5525 (1977).
13. H. B. Gray, A. W. Maverick, *Science* **214**, 1201 (1981).
14. A. F. Heyduk, A. M. Macintosh, D. G. Nocera, *J. Am. Chem. Soc.* **121**, 5023 (1999).
15. A. L. Odom, A. F. Heyduk, D. G. Nocera, *Inorg. Chim. Acta* **297**, 330 (2000).
16. In a N_2-filled glove box, $Rh_2^{0,II}(dfpma)_3Cl_2(CO)$ (185 mg, 0.230 mmol) was dissolved in 8 ml of THF and treated successively with cobaltocene (91 mg, 0.48 mmol) and triphenylphosphine (63 mg, 0.24 mmol). The solution turned red, with concomitant precipitation of yellow $[CoCp_2]Cl$. The mixture was filtered and the solvent removed in vacuo. The residue was redissolved in CH_2Cl_2 and filtered through a plug of Florisil. The volume was reduced to 5 ml and pentane was added. Cooling to –80°C overnight afforded the product as a yellow-orange microcrystalline solid (189 mg, 83% yield), which was characterized by satisfactory elemental analysis and by nuclear magnetic resonance (NMR) spectroscopy. ^1H NMR ($CDCl_3$) δ/ppm: 2.74 (s, 9H), 7.36 (m, 15H). ^{19}F NMR ($CDCl_3$) δ/ppm: –41.75 (d, $|^1J_{PF} + {}^3J_{PF}| = 1125$ Hz), –43.56 (d, $|^1J_{PF} + {}^3J_{PF}| = 1115$ Hz).
17. Small-scale photolysis experiments were carried out in high-vacuum cells comprising a 1-cm clear-fused-quartz cuvette and a 20-ml solvent reservoir isolated from each other and the atmosphere by Teflon valves. Spectroscopic grade solvent was dried and added to the cell by vacuum transfer. Hydrogen halide gases (HCl from the reaction of NaCl with H_2SO_4 and HBr from a lecture bottle) were freeze-pump thawed once before transfer into the cell. Irradiation was carried out on samples maintained at 15° to 20°C with the output of a 1-kW Hg/Xe lamp. The excitation light was passed through a distilled water filter (to remove infrared light) and appropriate neutral density and colored glass filters.
18. Large-scale photolysis experiments were performed in 100-ml custom high-vacuum quartz reaction tubes with a path length of ~2.5 cm. Sample preparation and irradiation are as in (*17*). After irradiation, the reaction solution was frozen, and noncondensable gas was passed through three U-traps maintained at 90 K and collected with a Toepler pump. The noncondensable gas was then combusted over hot CuO to confirm H_2 content.
19. Control experiments showed no production of H_2, as determined by Toepler pump gas collection. Irradiation of a 50-ml solution of 0.1 M HX (X = Cl, Br) in THF with light ($\lambda \geq 338$ nm) for 12 hours gave only an insignificant quantity of noncondensable gas ($\leq 2 \times 10^{-6}$ mol), which did not burn over CuO. Similarly, no H_2 was collected from solutions of $Rh_2^{0,0}(dfpma)_3(PPh_3)(CO)$ in THF containing 0.1 M HX maintained at 20°C in the dark for 12 hours.
20. I. S. Sigal, K. R. Mann, H. B. Gray, *J. Am. Chem. Soc.* **102**, 7252 (1980).
21. S.-S. Chern, G.-H. Lee, S.-M. Peng, *Chem. Commun.* **1994**, 1645 (1994).
22. K. R. Mann, M. J. DiPierro, T. P. Gill, *J. Am. Chem. Soc.* **102**, 3965 (1980).
23. A. L. Balch, M. M. Olmstead, *J. Am. Chem. Soc.* **101**, 3128 (1979).
24. Solutions of $Rh_2^{0,II}(dfpma)_3Cl_2(PPh_3)$ in THF containing 0.1 M HCl maintained in the dark at 20°C do not produce hydrogen as determined by Toepler pump collection of noncondensable gases. Moreover, isotopic scrambling involving the solvent is not observed. Photolysis of $Rh_2^{0,II}(dfpma)_3Cl_2(PPh_3)$ in d^8-THF containing 10 equiv of HCl results in the exclusive production of H_2 over the first 3 hours of irradiation, as evidenced by the appearance of a singlet in the ^1H NMR at 4.53 ppm (H_2). Continued irradiation gives subsequent formation of HD (δ = 4.50 ppm, $^1J_{HD}$ = 43 Hz), as expected from halogen trapping by d^8-THF to generate DCl. The deuterated acid then enters the photocatalytic cycle to produce HD and D_2.
25. C. Woodcock, R. Eisenberg, *Inorg. Chem.* **23**, 4207 (1984).
26. D. Evans, G. Yagupsky, G. Wilkinson, *J. Chem. Soc. A* **1968**, 2660(1968).
27. T. A. Albright, J. K. Burdett, M.-H. Whangbo, *Orbital Interactions in Chemistry* (Wiley-Interscience, New York, 1985).

28. Supported by a grant from the NSF (grant CHE-9817851).

30 May 2001; accepted 23 July 2001

Design of Bioelectronic Interfaces by Exploiting Hinge-Bending Motions in Proteins

David E. Benson,[1]* David W. Conrad,[1] Robert M. de Lorimier,[1] Scott A. Trammell,[2] Homme W. Hellinga[1]†

We report a flexible strategy for transducing ligand-binding events into electrochemical responses for a wide variety of proteins. The method exploits ligand-mediated hinge-bending motions, intrinsic to the bacterial periplasmic binding protein superfamily, to establish allosterically controlled interactions between electrode surfaces and redox-active, Ru(II)-labeled proteins. This approach allows the development of protein-based bioelectronic interfaces that respond to a diverse set of analytes. Families of these interfaces can be generated either by exploiting natural binding diversity within the superfamily or by reengineering the specificity of individual proteins. These proteins may have numerous medical, environmental, and defense applications.

Hybrid devices consisting of biological and abiotic components combine the exquisite molecular recognition properties and complex activities of biomolecules with the power of existing electrochemical (*1–6*), optical (*7–12*), magnetic (*13, 14*), or mechanical (*15*) technologies. Central to the development of such devices is the construction of interfaces that transduce biomolecular events such as ligand binding into abiotic signals (*6, 16*) or actions (*17, 18*). Ideally, it should be possible to build families of biomolecular interfaces that respond to a wide variety of chemical stimuli (*19*). A biomolecular interface comprises three different functions: molecular recog-